CHALMERS
UNIVERSITY OF TECHNOLOGY

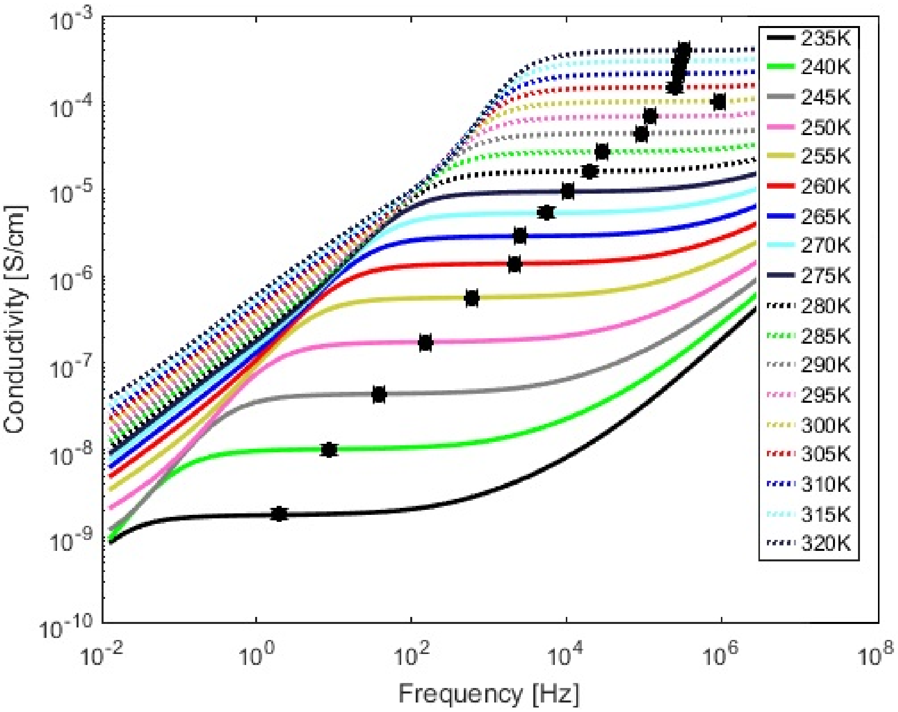

Conductivity and Relaxation in Polymer Based Solid Electrolytes

Master's thesis in Applied Physics

MANSOUREH SHOJAATALHOSSEINI

Department of Physics
CHALMERS UNIVERSITY OF TECHNOLOGY
Gothenburg, Sweden 2016

Master's thesis 2016

Conductivity and Relaxation in Polymer Based Solid Electrolyte

MANSOUREH SHOJAATALHOSSEINI

Department of Physics
Condensed Matter Physics
Chalmers University of Technology
Gothenburg, Sweden 2016

Conductivity and Relaxation in Polymer Based Solid Electrolyte
MANSOUREH SHOJAATALHOSSEINI

Supervisor: Professor Jan Swenson, Division of Condensed Matter Physics
Examiner: Professor Jan Swenson, Division of Condensed Matter Physics

Master's Thesis 2016
Department of Physics
Division of Condensed Matter Physics
Chalmers University of Technology
SE-412 96 Gothenburg

Conductivity and Relaxation in Polymer Based Solid Electrolyte
MANSOUREH SHOJAATALHOSSEINI
Department of Physics
Chalmers University of Technology

Abstract

Lithium ion batteries have received much attention as rechargeable batteries due to their high energy and power density. One way of satisfying the safety conditions required for Li-ion batteries is the use of solid polymer electrolytes (SPE) as opposed to the conventional liquid electrolytes. SPEs eliminate the shape limitation and overcome problems related to leakage and flammability. Different polymer electrolyte systems have been extensively studied. PEO- LiX, as used as the base polymer electrolyte in the present study, is one of these systems. In this study we have used lithium bis(trifluoromethanesulfone)imide (LiTFSI) as the salt, Al_2O_3 as the nanofiller and poly(ethylene oxide) (PEO) as the polymer. Samples of different molar ratios of PEO/ Li, 16:1 and 8:1 have been prepared. The obtained polymer electrolyte films have thicknesses of 100-150 μm. The major drawback of this PEO-Li system is its relatively low conductivity at room temperature. Since the ionic conductivity of the polymer electrolyte occurs in the amorphous phase of the polymer, the semicrystalline character of PEO below its melting point at 60°C is detrimental for the ionic conductivity. Various methods have been applied to suppress the crystallization, such as adding nanoparticles or ionic liquids. In this project we used 1-butyl-3 methylimidazolium bis(trifluoromethanesolfonyl)imide (BMITFSI) to enhance the ionic conductivity and reduce the crystallization. The ionic conductivity and relaxation processes of the system have been studied by dielectric spectroscopy (DS) and, furthermore, thermal properties, such as glass transition and melting temperature of the polymer, have been determined by differential scanning calorimetry (DSC). The results show that the introduction of the ionic liquid speeds up the segmental polymer dynamics, but only to concentrations of about 20 wt%, despite that the ionic conductivity increases further (to above 10^{-4} S/cm at 300 K) at higher concentrations of the ionic liquid. Thus, it is evident that the motion of the Li ions decouples from the segmental polymer dynamics at higher concentrations of the ionic liquid and instead becomes more dependent on the viscosity of the ionic liquid.

Key words: Solid polymer electrolyte, PEO, ionic conductivity, ionic liquid.

Acknowledgements

First, I would like to thank my supervisor and examiner professor Jan Swenson for his guidance during this thesis.

I would also like to thank all the members in KMF group for their support.

My special thanks go to my mother, Sedigheh Hosseini, for her love and her encouraging me to believe in myself. Last but not least I would like to thank my sisters, without them I would not be able to do anything.

Mansoureh Shojaatalhosseini, Gothenburg, 2016

Contents

List of Figures

List of Tables

1

Introduction

In today's world, reducing carbon dioxide emissions plays a crucial factor in facing the challanges of climate change. Storing energy in batteries provides a successful solution for global energy needs as it facilitates the incorporation of renewable energy sources such as solar and wind power, and also provides an alternative to fossil fuels in car. In this contex, battery technology has rapidly evolved since the last century. Batteries are classified into primary and secondary types: in primary, or non-rechargeable, chemical reactions cannot be reversed, such as in alkaline and zinc- carbon batteries. In secondary, or rechargeable batteries, redox reactions can be reversed. Nickel- cadmium, lead acid batteries and lithium ion batteries belong to this category [1-2]. Lithium ion batteries have been extensively studied in both research and industry for the last decades. An impetus to create this type of battery is the significant dependence in our daily lives on portable devices such as smartphones, tablets, and laptops. Lithium-ion batteries have several advantages over the lead - acid batteries. Also, they are a promising alternative for electric power application. Higher volumetric (Wh/L) and gravimetric (Wh/kg) energy densities of lithium ion batteries have made them more appealing compared to other conventional battery systems [3-4]. Indeed, their lifetime and energy efficiency represents an ideal power source for portable battery devices and hybrid electric vehicles. Most batteries contain liquid electrolytes, and are not suitable for some applications due to safety hazard. Research to meet the safety conditions emphasizes the importance of using solvent free or dry electrolytes and solid polymer electrolytes (SPE). Replacing liquid electrolytes with solid polymer electrolytes (SPE) carries more advantages. They overcome problems related to leakage, short circuits and flammability. SPEs eliminate shape and size limitations in batteries, which traditionally come in cylindrical shape. Conventional SPEs, are membranes based on polymer host structures which are prepared by blending a polymer type of poly-ethylene oxide and polypropylene oxide with a suitable ionic salt. Since a high ionic conductivity is a key requisite for SPEs it is common to add a liquid organic solvent to the polymer-based electrolyte [5-6]. Improving the electrolyte's ionic conductivity requires knowledge of chemistry. There are some reported methods to enhance the ionic conductivity by adding ceramic powders and nanoscale particles. Developing electrolyte systems, including IL, is also an effective method for obtaining a sufficiently high conductivity at an ambient temperature. In all methods mentioned above it has been attempted to develop electrolytes aiming to improve mechanical properties, electrode compatibility and low temperature conductivity. Difficulties related to other properties such as light weight, compactness and simple manufacturing are also worth discussing. Although tremendous developments have been reached in the field of these types of electrolytes, Li-ion batteries still have some undesirable characteristics.

In this thesis, after a brief introduction on basic concepts about batteries and polymer electrolytes (PE), a classification of PEs is made. Different types of polymer based electrolytes are also explained. Additionally, the roles of all components are described to give an overall understanding of the concept of PEs. In the experimental chapter, the materials used, the sample preparation processes, and some theory behind the applied techniques (differential scanning calorimetry and dielectric spectroscopy) are outlined. Moreover, the interpretation of data, analysis of results and the effects of the ionic liquid (IL) in polymer films are discussed. Finally, the last chapter includes a conclusion and suggestions for future work on these types of polymer films.

1.1 Objective

The purpose of this thesis is to develope room temperature polymer electrolytes for lithium ion batteries with an acceptable range of ionic conductivity. The main focus is ionic conductivity. In addition, the effect of the ionic liquid on relaxation dynamics, thermal and electrical properties of the electrolyte systems are investigated. Systems consisting of PEO - LiTFSI, with different ratios of a polymer-salt (8:1, 16:1), were synthesized. Then, various concentrations of ionic liquids were blended to achieve the optimal system.

2

Theoretical Considerations

Here, a brief explanation of the structure and operation of lithium ion batteries is given. In the following section, some related conceptions such as glass transition temperature (T_g), relaxation time (τ), and ionic conductivity (σ), are brought up. Furthermore, the relation between these parameters and their effects on ion diffusion, which determines the electrolyte performance, are presented.

2.1 Lithium-ion Batteries

The developement of lithium ion battery systems began in 1980. However, the first commercial lithium ion batteries were offered by Sony in the 1990s. Since then, a large number of these types of batteries have been produced due to a growth in demand. Subsequently, many research groups have attempted to improve the power density, safety, cost, and other desired aspects [7]. Lithium ion batteries function from the transfer of Li ions between two electrodes. Li^+ moves from the anode to the cathode during discharge, where oxidation occurs, and while charging, Li^+ is reduced and lithium ions move from the cathode to the anode, hence the process is reversible. Two key properties of electrodes are permiting the insertion and extraction of lithium ions, and also the ability of electron acceptation, to compensate for the consumed electrons and balancing the reaction. The external circuit connected to the electrodes and the difference in potential between the two electrodes, is the reason why the electrons are circulating [8]. The Gibbs free energy, which drives the system to a stable condition, can be calculated as follows:

$$\Delta G = \text{-nF} E_{cell} \tag{2.1}$$

where n is the number of electrons, F is Faraday's constant, and E_{cell} is the electrochemical potential difference. Lithium, which is a light element (6.94 g/mol), has the lowest oxidation number and highest electrochemical potential. In addition, it can be managed safely. Compared to lead-acid batteries, lithium ion batteries are less sensitive to high temperatures, have less deposition in charge and discharge processes and are lighter in weight [9]. The main disadvantage is the higher cost. A lithium ion battery is schematically illustrated in Figure 2.1, which includes an anode, cathode and electrolyte. The transportation of ions occurs in the electrolyte.

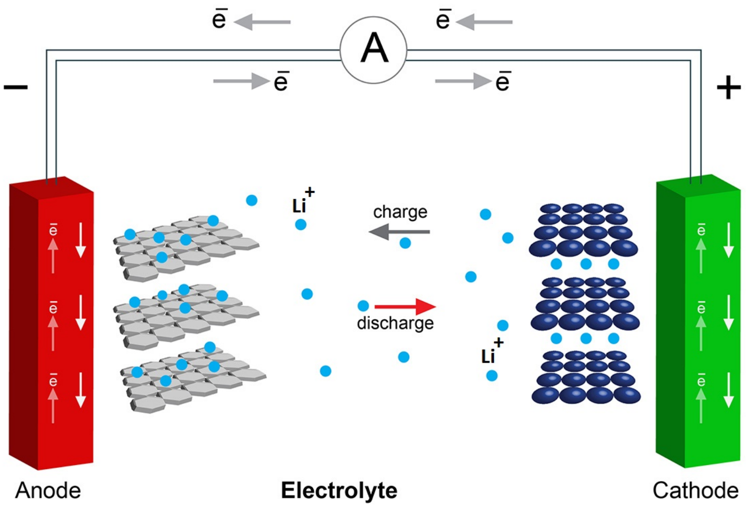

Figure 2.1: Schematic illustration of a Li-ion battery

2.2 Glass Transition

In general, molecular arrangements in materials can be classified into ordered and disordered arrangements, which exist in fluids, glasses, and crystalline states. Above the melting point T$_m$, a liquid always remains a liquid and below T$_m$, it emerges as a supercooled liquid, as a glass (depending on the temperature) with a disordered arrangement of molecules, or as a crystal with ordered molecules in a regular lattice. Whether they end up in glass or crystal form depends on the cooling rate and how easily the liquids crystallize. When a liquid cools slowly, the molecules have time to rearrange and receive a low potential energy, generally resulting in crystallization. If cooling occurs fast enough, the crystallization will be mitigated and the glass state will prevail below the so-called glass transition temperature T$_g$. Below T$_m$, the liquid becomes supercooled, and as soon as the viscosity of the supercooled liquid passes the value equal to 10^{13} poise ($1P = 1g \cdot cm^{-1} \cdot s^{-1}$), the amorphous glass state appears. Then, the transition temperature from the supercooled liquid state to the solid state is defined as the glass transition temperature (T$_g$). T$_g$ gives the temperature where the segmental polymer relaxation time is roughly 100 seconds.

Within the glassy state, properties such as density and entropy slightly change. T_g is, however, dependent on heating and cooling rates [10]. Figure 2.2 shows temperature-volume curves and T_g shifts to a lower temperature with a decreasing cooling rate. The increasing viscosity with a decreasing temperature, is commonly described by the Vogel-Fulcher-Tammann (VFT) equation:

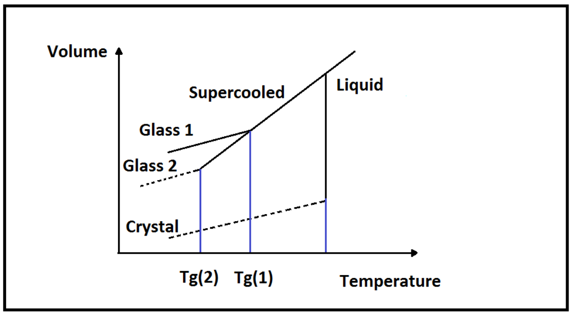

Figure 2.2: Different cooling rates result in T_g (1) and T_g (2)

$$\eta = \eta_0 \cdot exp\left(\frac{-DT_0}{T - T_0}\right) \tag{2.2}$$

where η_0 is the extrapolated value of viscosity to infinite temperature, η_0 is $\sim 10^{-4}$ poise, T_0 is the value where the viscosity η extrapolates to infinity and D is the so called fragility parameter, which describes the derivation from an Arrhenius temperature dependence. The main relaxation in polymers, related to the segmental motion of the main chain, is the α relaxation. τ_α increases by decreasing temperature in the same way as the viscosity. Therefore, its relaxation time also shows a non-Arrhenius temperature dependence

$$\tau_\alpha = \tau_0 \cdot exp\left(\frac{-DT_0}{T - T_0}\right) \tag{2.3}$$

where τ_α is the relaxation time at temperature T and τ_0 is the extrapolated value of the relaxation time to infinite temperature. According to this equation, polymer systems can be classified as fragile, when a pronounced non-Arrhenius temperature dependency of τ_α exists (This corresponds to a low value of D). In this case, τ_α and the viscosity of the liquid rapidly increases close to a value of T_g. In contrast, when an Arrhenius temperature dependency is observed (a high value of D), the supercooled liquid is classified as strong.

Other types of relaxation processes in polymers are described as β-relaxation and γ-relaxation, which are observed below T_g. β-relaxation can be related to the motion of the polymer segments close to ether oxygens coordinated to Li^+ ions or close to crystalline regions. The γ-relaxation is based on the local twistings of chain ends and local intramolecular movement of the ethylene groups. Both relaxations are faster than the α-relaxation [11].

2.3 Ionic Conductivity

The ionic conductivity of a solid polymer electrolyte is related to the segmental motions of the polymer chains and the number of mobile ions. The ionic conductivity can be expressed as follows:

$$\sigma = \sum_i n_i \cdot q_i \cdot \mu_i \tag{2.4}$$

where, n_i is the charge concentration of both positive and negative charges, q_i is the charge and μ_i is the ion mobility. The unit for ionic conductivity is Scm^{-1}, where S is Ω^{-1}. It is evident that the ionic mobility is promoted by a lowering of T_g, since this leads to faster segmental motions of polymer chains at a given temperature, therefore, also faster diffusion of ions. Although the total mobility involves the mobility of both positive charges (μ_+) and negative charges (μ_-), only the conduction of cations is effective in the case of Li- electrolytes [12]. The ionic conductivity within the amorphous regions is temperature dependent and can be approximated by the Vogel-Tammann-Fulcher (VTF) relation

$$\sigma = \sigma_0 \cdot exp\left(\frac{-B}{T - T_0}\right) \tag{2.5}$$

where, σ_0 is the pre-exponential factor and T_0 is the temperature, where σ goes to zero [6]. Methods used to reach higher conductivity in polymer electrolytes, and thereby an enhanced battery performance, are mostly associated with a loss of mechanical properties and compatibility, which, in turn, decrease the battery cycle life.

3

General Classification of Polymer Based Electrolytes

In this chapter, different types of polymer electrolyte systems are described. Also, the general concept of introducing salts, ionic liquids and nanofillers to polymer electrolytes, is explained.

3.1 Polymer Electrolytes

Electrolytes are an inert transport medium for mobile ions, and therefore, an important component in batteries. High ionic conductivity, mechanical and thermal stability, durability, and the use of non-toxic and renewable materials are some desired characteristics of electrolytes. Polymer electrolytes can be classified into liquid, gel, solid polymer, and ionic liquid electrolytes. Liquid electrolytes generally have high ionic conductivity, but suffer from safety issues and the absence of mechanical stability. Polymer electrolytes relieve these problems and, in addition, their flexibility and easy manufacturing are attractive characteristics. Flexibility of polymer chains assists in the efficient ion transport of a salt dissolved in the polymer. Polymer electrolytes are therefore also suitable for other technological applications, such as in fuel cells and capacitors. Some required properties for polymer electrolytes are listed, such as high ionic conductivity, close to liquid electrolytes ($\sigma \geq 10^{-4} Scm^{-1}$), large voltage windows and long cycle-life. Also, compatibility with used material in electrodes is known as an important point. Despite low ionic conductivity, which is an undesired trait in polymer electrolytes, still the majority of requirements are met for battery application [13].

3.2 Classification of Polymer Electrolytes

In the 1970s, ion conducting polymeric materials were discovered, and the first synthesis of polymer electrolytes were subsequently introduced. Since then, various polymer electrolyte systems, such as plasticized polymer-salt electrolytes, polymer gel electrolytes, rubbery electrolytes, and composite polymer electrolytes, have been introduced [14].

3.2.1 Solid Polymer Electrolytes

High molecular weight polymer electrolytes can be obtained by mixing poly(ethylene oxide) (PEO) or poly(propylene oxide) (PPO) with Li-X (where X defines a charge delocalized anion) salt. By blending different types of ionic salts, different transporting ions such as Li^+, K^+, Mg^+, Na^+ can be extracted. Lithium ions are highly attractive due to their considerable capability of receiving a higher range of conductivity at lower temperatures in comparison to other polymer electrolytes, and they also reduce dendrite in lithium electrodes. Polymer electrolytes of PEO are typically semi-crystalline below their melting temperature around $60°C$. As it is known, the function of the amorphous phase in this type of system depends on the salts content, as well as the preparation method. At ambient temperature, the ionic conductivity is reduced, due to the presence of crystalline phases below $60°C$, which prevent the ion transport. Reported common conductivities range between 10^{-8} Scm^{-1} and 10^{-4} Scm^{-1} at temperatures in the range of $40°C$- $100°C$. It is worth mentioning that some research groups recently investigated the ionic conductivity related to the crystalline region in (PEO) : $LiAsF_6$, and the conductivity is approximately half of that of the amorphous region. To achieve higher conductivity at a lower temperature and to spur ion transport, materials with lower T_g are attractive [15]. Figure 3.1 shows Li ions transport mechanism in a polymer. Ion conductivity in this system is an effect of segmental motions of the host polymer. This assists in creating a suitable coordination with respect to ions where the ether oxygen in polymer chains have an inclination to attract the cation and wrap around Li^+. This will create temporary bonds and then ions will be dissociated from their position into the next sites. Strong interaction between polymer-cations results in further dissolvement of the salt, but it reduces the movements of the cations [16]. Therefore, fast ion transport requires segmental motions and relatively weak cation coordination to the polymer chains. It is worth mentioning that very high concentrations of

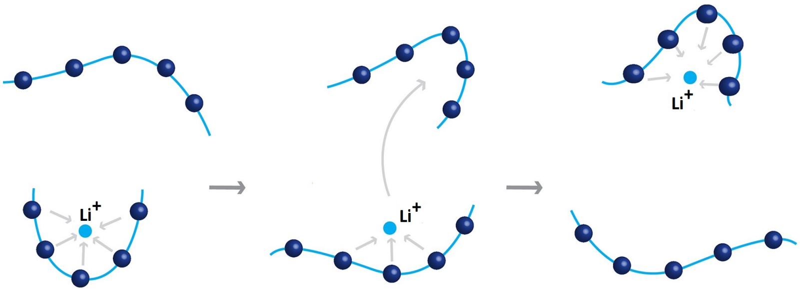

Figure 3.1: Schematic of lithium ion motion in polymer (PEO)

Li-X in order to provide more numbers of ions, leads to less mobility (of ions) due to aggregation of ions.

3.2.2 Gel Polymer Electrolytes

Gel polymer electrolytes (GPEs) are a second category of polymer electrolytes. However, they are neither categorized as liquid nor solid polymers. They have high ionic conductivity, close to that of liquid electrolytes, and superior safety compared to liquid electrolytes. The reported value of conductivity is in the range of 10^{-4} - $10^{-3} Scm^{-1}$. Poor mechanical strength is a disadvantage which can be improved by adding components to create cross-linking of polymers. Among polymers, poly (vinylidene fluoride) (PVdF), poly (methyl methaacrylate) (PMMA), and poly (vinyylidene fluoride-hexafluoroproplene) (PVdF-co-HFP) have been used as polymer hosts [17-18].

3.2.3 Plasticized Polymer Salts

Solid polymer electrolytes are characterized by a low value of conductivity. One way to enhance the ionic conductivity and obtain an acceptable value, is by mixing SPEs with liquid plasticizers. Plasticizers improve the polymer's flexibility. They facilitate the segmental motions and assist in reducing the crystallinity. It is likely that in polymer- plasticizer linkage, intramolecular coordinations are more effective in creating conductivity pathways for Li^+ [19-20].

3.2.4 Rubbery Electrolytes

A rubbery electrolyte with a low glass transition temperature is obtained by adding a big amount of salt into a polymer. This type of electrolyte is characterized by a high conductivity, which is explained by the fast motion of ion clusters (aggregation due to high ratio of salt with respect to polymer) in the electrolyte. Low electrochemical stability is regarded as a disadvantage for this type of electrolyte [13].

3.2.5 Composite Polymer Electrolytes

Composite solid polymer electrolytes (CSPEs) have received the attention of many research groups, however, the initial idea is not new. CSPEs are solid polymer electrolytes synthesized by micro- or nano-sized fillers to enhance the morphological properties by hindering the crystallization. The presence of nanofillers can also speed up the segmental polymers dynamics and subsequently create a greater ion transfer, leading to a further enhancement of the conductivity. Using nanofillers instead of plasticizer improves the compatibility of the electrolyte with the electrodes [21-22].

3.3 Salt

Salts should be stable in terms of electrochemical and thermal properties, as no reaction with electrodes are desired. Salts should have high solubility and low interaction with the polymer host to provide a higher number of mobile Li ions, in order to raise the conductivity. Furthermore, selecting a non-toxic salt and one that is complatible with the environment are factors which, are of importance. Although, most types of salts fail to fulfill these properties. Litiumperklorat ($LiClO_4$), Lithium hexafluoroarsenate ($LiAsF_6$), Lithium bis(oxalate)borate (LiBOB), and Bis(trifluoromethane)sulfonimide lithium salt (LiTFSI) are commonly used in lithium batteries. However $LiAsF_6$ is toxic, $LiClO_4$ is highly oxidant, and LiBOB has a lower degree of solubility. LiTFSI has proven to be a practical salt in polymer electrolytes. A negative effect of adding a salt is a reduction in the internal flexibility of the polymer, which unfortunately is detrimental for the conductivity [23-24].

3.3.1 Dissolving Salts

The basic mechanism of a salt dissolving Li-X in polymers is the changes in entropy (S) and enthalpy (H), which will affect the Gibbs free energy (ΔG).

$$\Delta \mathrm{G} = \Delta \mathrm{H} - \mathrm{T}\Delta \mathrm{S} \tag{3.1}$$

Dissolving a salt into a polymer is favourable when the Gibbs free energy is negative. The entropy is increased due to the disarrangement of the ions in the salt, and, when breaking up the crystal lattice, this entropy is positive. However, the coordination of salt ions to the polymer leads to a stiffening of the polymer chains, which gives a negative entropy contribution. The positive enthalpy changes are due to the lattice energy of salt, and the negative enthalpy changes are caused by the interaction between the salt and the solvent. In order to increase the dissociation of salt in the polymer, it should have a low lattice energy [25]. Lattice energy depends on the size of the ionic radii, which implies that salts of smaller size have a lower lattice energy. In addition to a high dielectric constant, polymers inhibit ion-ion interactions and avoid aggregation of ion pairs. However, such polymers exhibit higher T_g, which results in lower mobility of polymer chains [26].

3.4 Ionic Liquids

Ionic liquids(ILs) are pure salts which have a melting point below $100°C$ and the term room temperature ionic liquid (RILs) is used when they are liquid, even at room temperature. ILs are defined as a new class of materials, however the first compound of ILs, ethanol ammonium nitrate, was introduced in 1887 by Gabriel [27]. Their compatibility with the environment is why they are referred to as green solvents. Their unique physical property allows them to be used instead of volatile organic and hazardous solvents. ILs consist of organic anion and organic/inorganic asymmetric cation solutions. The low melting point of ILs is due to the asymmetrical cations, which prevent cations and anions from arranging into a crystal lattice, unlike traditional salts which are able to pack into a crystal lattice. Due to the possibility of designing ILs by selecting various cations and anions, they have been named designer solvents. The most common anions are BF_4^{-1}, PF_6^{-1} and TFSI, and in general, cations are based on immidazolium, sulphonium and phosphonium. Some properties include low vapour pressure, non-flammability, good solubility, high oxidative stability, and the ability to operate in a wide range of temperatures [28-29]. Many ILs are stable above $300°C$, which allows high temperature operation. Furthermore, due to their thermal stability and high conductivity, the interest for using ILs in electrochemical cells and devices, sensors and fuel cells, has increased. Recently, electrolytes based on ILs, where the electrolyte is replaced by ILs or by the addition of ILs into PEO-LiX electrolytes, have been investigated in order to improve the ionic conductivity. The high cost of ILs is considered as a significant disadvantage [30].

3.5 Nanofillers

Among polymer electrolytes, PEO-LiX has been most studied. Despite its low conductivity, it is favourable as an electrolyte system, as explained in section 3.2.1. Therefore, in order to enhance the conductivity, adding plasticizers is recommended, which, as aforementioned, causes the reduction of mechanical properties or unwanted reactions with the electrodes. This results in losing the battery´s safety. Hence, many research groups have searched for methods to increase the conductivity with minimum damage of the electrolyte's quality. As a solution, inert nano fillers such as SiO_2, Al_2O_3 and TiO_2 have been employed [31]. Nanoscale fillers facilitate the maintenance of the amorphous phase due to a large surface area, which prevents the reorganization of polymer chains and crystallization. Therefore, lower, more practical temperatures of electrolytes can be achieved. Some articles explain cross linking effects of nanoparticles, where nanofillers act as cross linking centres for segments of the polymer chains and modify the coordination of ions, leading to a facilitated motion of Li^+. Also, it is worth noting that the Lewis-acid property of nano-fillers against ether oxygens assists Li ion separation [32-33]. In addition, some studies infer that polymer chains have a tendency to curl around the nanoparticles, even if the interaction between nanoparticles and polymer chains are nonatractive. Thus, the free volume around polymer chains increases and facilitates the movement of the Li^+ ions [34].

3.6 Polymer's Morphology

Based on different molecular structures, polymers are categorized into amorphous and semi-crystalline polymers. Amorphous polymers are the polymers which do not crystallize below their melting point; therefore, with cooling, they remain in the supercooled state, which at a lower temperature is followed by an amorphous state. However, some polymers can crystallize, but it can be avoided by not giving them the required time to crystallize. A two-dimensional schema of an amorphous (on the right) and semi-crystalline polymer (on the left) is shown in figure 3.2. In amorphous polymers, the polymer chain arrangement is random. In other words, branches and pendant groups of polymer chains cannot pack orderly. Generally, amorphous polymers are softer than semi-crystalline polymers, which have both crystalline and amorphous regions. They are typically composed of $40-70$ percent amorphous polymers. The percentage of crystallinity affects the properties of the polymer. The incorporation of the strength property of crystalline polymers with the flexibility of amorphous polymers, has made semi-crystalline polymers more attractive for a wide range of applications.

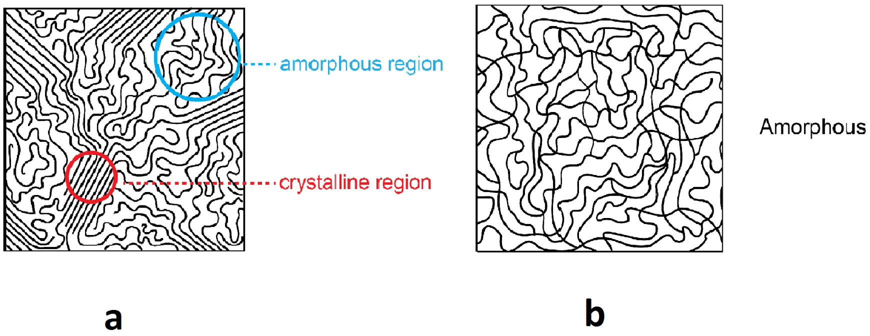

Figure 3.2: Two dimensional schematic of semi- crystalline (a) and amorphous (b) polymer

In polymers, T_g is affected by the polymer chain stiffness, which is based on the crosslinking and the structure of the polymer's backbone. Flexibility of the main chain assists in reaching a lower T_g. Intermolecular forces and higher molecular weight increase T_g [35-36].

4

Materials

Polyethylene oxide (molecular weight 6×10^6 g/mol) from Polysciences Inc and Lithium bis(trifluoromethanesulfonyl)imide (LiTFSI) salt of high quality (99.95% purity) from Aldrich, Al_2O_3 nanofiller with 20 nm particle size from Degussa and ionic liquid (IL), 1-Buty-3- methylimidazolium bis(trifluoromethylsulfonyl) imide (BMITFSI), from Sigma Aldrich, were used as starting materials.

4.1 Polymer - Poly(ethylene Oxide) (PEO)

High molecular weight poly(ethylene oxide) PEO is known as the most typical polymer host to construct the electrolyte. This is caused by its good solubility, which is due to its sufficient electron donor ability where the main chain molecule -CH_2-CH_2-O- dissolves the salt better than other polymers. PEO has poor conductivity and is a semi crystalline polymer with $60-80\%$ crystallinity below its melting temperature of about $60°C$. For a polymer based electrolyte (PEO -LiX complex), the degree of crystallinity depends on the ratio of EO/Li, which describes the number of ether oxygens per Li- ion [37].

4.2 Salt - LiTFSI

Lithium bis(trifluoromethanesulfone)imide (LiTFSI) salt, with white powder appearance, is used to provide Li-ion conducting species to the electrolyte. It is very interesting due to its chemical and thermal stabilities; moreover, it is very soluble in most solvents and it exhibits desirable safety battery performance. LiTFSI is a large organic salt with a bulky anion, which suppresses crystallization [38]. The chemical structure of LiTFSI is shown in figure 4.1 and table 4.1 shows some properties of this salt.

Table 4.1: Properties of LiTFSI

Linear Formula	$(CF_3SO_2)_2NLi$
Molecular Weight (g/mol)	287
Melting point (K)	509

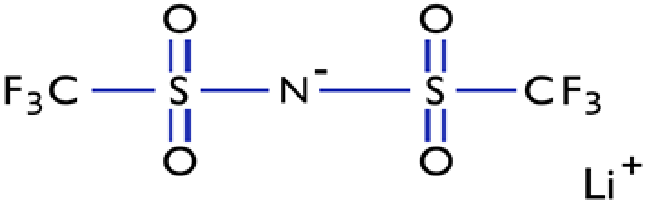

Figure 4.1: Chemical structure of LiTFSI

4.3 Ionic Liquid - BMITFSI

The ionic liquid, 1- Butyl-3-methylimidazolium bis (trifluoromethylsulfonyl)imide, BMITFSI, is used to prepare the sample. It consist of bis(trifluoromethylsulfonyl) imide as anion and 1-Butyl-3-methylimidazolium as cation. BMITFSI is hydrophobic, but has good miscibility in methanol, accetonitrile and acetone. The most common application of this IL is found in electrochemistry and energy storage such as lithium batteries and supercapacitors [39]. The chemical structure of BMITFSI is shown in figure 4.2 and table 4.2 shows some properties of this ionic liquid.

Table 4.2: Properties of BMLiTFSI

Linear Formula	$C_{10}H_{15}F_6N_3O_4S_2$
Molecular Weight (g/mol)	419
Melting point (K)	269

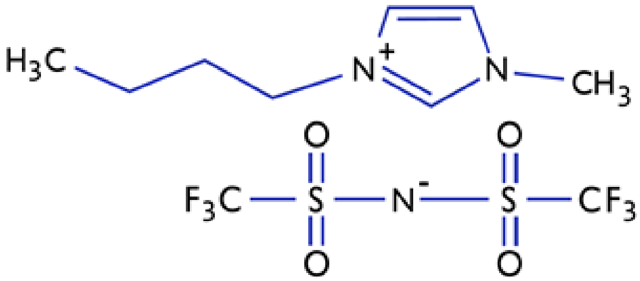

Figure 4.2: Chemical structure of BMITFSI

4.4 Nanofiller - Alumium Oxide

Al_2O_3 is an inorganic nanofiller with a particle size equal to 20 nm in this work, which enhances the electrolyte performance due to the presence of a large surface area between the polymer and nanofiller. It prevents the crystallization of the PEO and improves the ionic conductivity.

5

Methods

In the following chapter, two methods to prepare polymer electrolytes (PEs) are described. A detailed description of the sample preparation of the polymer film is given.

5.1 Common methods to prepare PE

Common procedures for polymer electrolyte film preparation include solution casting techniques and hot press methods. Casting methods are recognized as a traditional procedure when making polymer films. A suitable amount of salt and polymers are dissolved in a solvent and stirred for adequate time until the solution is dissolved. In the case of composite polymer films, nano particles are added during magnetic stirring. Afterwards, the solutions are casted in a petri dish and dried in a vacuum oven. The thickness of the film is $100\mu m$ - $200\mu m$. Hot press casting, which is presented by Gray et al [15], is identified as a faster method, and the prepared polymer electrolytes are dried completely. In this method, a polymer powder, salt and nano/micro particles are physically mixed. The mixed powder is heated to a temperature above the melting temperature of the polymer host. The obtained mixture is placed between two metal plates or twin rollers. The obtained polymer electrolyte film has a thickness of 100μm- 600μm.

5.2 Sample Preparation

In this work, all samples were prepared by solution casting. Polymer films were prepared with, and without, an ionic liquid; PEO-LiTFSI-nanofiller electrolyte films, and PEO-LiTFSI- BMITFSI(X)- nanofiller electrolyte films respectively.

5.2.1 PEO-LiTFSI-Nanofiller Film

The electrolyte film was prepared by first blending a calculated amount of Al_2O_3 fillers in acetonitrile. Then, it was treated with ultrasonic waves for 4-5 hours to obtain a homogenous solution. After that, the polymer (PEO) was added intently in small amounts to avoid agglomeration. The desired homogenous solution was vigorously stirred under magnetic stirring for 2 days (48 h). LiTFSI salt was mixed in the solution and stirred for 2-3 hours. The resulting solution was cast onto the PTFE dishes, and afterwards these dishes were put in a box with molecular sieves located to facilitate the evaporation of acetonitrile and the removal of the solvent. Samples were put in a vacuum oven for 1 day at a temperature equal to 333 K, to remove the residual moisture. Then samples were transported into an argon filled glove box. Afterwards, the films were pulled out from the petri dishes and placed between brass electrodes for dielectric measurements. Two types of films with a thickness of 100μm - 150μm, with various ratios of EO/Li, corresponding to 16 and 8 monomeric units of ethylene oxide (CH2CH2) per Li-ion, were prepared.

5.2.2 PEO-LiTFSI- BMITFSI(X)-Nanofiller Film

The appropriate amount of nanofiller was dissolved in acetonitrile. The polymer was added, according to the procedure explained in 5.2.1; the solution was stirred for 1 day, followed by the addition of the ionic liquid BMITFSI. Homogenous solutions were kept under stirring (1200 pmr/min) for 1 day. The LiTFSI salt was mixed, and after 2-3 hours slurry solutions were cast in petri dishes. Petri dishes were placed in a box with molecular sieves for 2 days to dry slowly, and were kept in a vacuum oven for 1 day at a temperature equal to 333 K. The polymer composite films were prepared with the two of EO/Li ratios (16:1 and 8:1), and the weight fractions 10, 20, 30 and 40wt% IL in the case of 16:1 and 20wt% IL in the case of the higher salt content 8:1. These weight fractions give the weight of the IL relative the weight of PEO-LiTFSI.

6

Experimental Techniques

To determine the ionic conductivity and relaxation processes, dielectric spectroscopy (DS), also known as impedance spectroscopy was used. To find the thermal properties of the samples, differential scanning calorimetry (DSC) was used. The information obtained from both methods gives us a desired knowledge about the dynamics in the materials. Both techniques and the theory behind them are explained in this section.

6.1 Dielectric Spectroscopy

Dielectric spectroscopy is a versatile technique due to its wide frequency range. A measurement is based on the dielectric properties of the sample against an alternating electric field. In general, the dielectric response of the material is related to the permittivity; its ability to polarize when an external electric field is applied. In fact, the presence of an electric field affects the electrons' distribution around the nuclei and causes the electron cloud to be shifted from the nuclei, resulting in polarization. This mechanism is described by three types of polarizations: electric polarization related to charge motion from their original positions, atomic polarization related to the distortion of their atomic positions, and orientational polarization, which exists in polar molecules and is related to the reorientation of dipoles with respect to an electric field [40-41].

Polarization produced by an electric field is given by

$$\mathbf{P} = (\epsilon_r - 1)\epsilon_0\mathbf{E} \ , \quad \epsilon_r = \frac{\epsilon}{\epsilon_0} \tag{6.1}$$

where ϵ_0 is the permittivity of free space and ϵ_r is the permittivity of the material. Then, the electric displacement field is defined by

$$\mathbf{D} = \epsilon_r\epsilon_0\mathbf{E} \tag{6.2}$$

By using a time dependent electric field

$$\mathbf{E}_w(t) = E_0 exp(i\mathbf{w}t) \tag{6.3}$$

a modulated electric displacement is induced

$$\mathbf{D}_w(t) = D_0 exp(i\mathbf{w}t - i\delta(\mathbf{w})) \tag{6.4}$$

amplitude D_0 and phase difference $\delta(\mathbf{w})$ depend on the electric properties of the material.
Equations (6.3) and (6-4) can be adapted to obtain ϵ^*.

$$\frac{\mathbf{D}(w)}{\epsilon_0 \mathbf{E}(w)} = \epsilon' - \epsilon'' = \epsilon^* \tag{6.5}$$

where ϵ' is the real part and ϵ'' is the imaginary part of the complex permittivity. The Kramers- kronig relation describes how the real part and imaginary part of ϵ^* are related to each other.

$$\begin{aligned} \epsilon'(w) &= 1 + \frac{2}{\pi} P \int\limits_0^\infty \frac{\nu \epsilon''(\nu)}{\nu^2 - w^2} d(\nu) \\ \epsilon''(w) &= \frac{2w}{\pi} P \int\limits_0^\infty \frac{\epsilon'(\nu) - 1}{\nu^2 - w^2} d(\nu) \end{aligned} \tag{6.6}$$

Applying a modulated voltage and current through the sample gives us the possibility to measure the complex impedance Z^* and, consequently, it gives the complex permittivity. Since the result of the measurement is expressed in form of complex permittivity it requires further steps to obtain a final expression. Figure 6.1 shows the schematic of the circuit used in dielectric spectroscopy. Complex impedance $Z^*(w)$, can be obtained by knowing the resulting sample potential and the sample current, as follows:

$$Z^* = \frac{V_s^*}{I_s^*} exp(i\phi) \tag{6.7}$$

Where $V_s^*(t)$ and $I_s^*(t)$ can be written as:

$$V_s^*(t) = V_0 exp(iwt) \tag{6.8}$$

$$I_s^*(t) = I_0 exp(iwt + i\phi) \tag{6.9}$$

In addition, complex permittivity ϵ^* can be derived from the measured impedance of the sample by using the following equation:

$$\epsilon^*(w) = \epsilon' - \epsilon'' = \frac{-i}{wZ^*C_0} \tag{6.10}$$

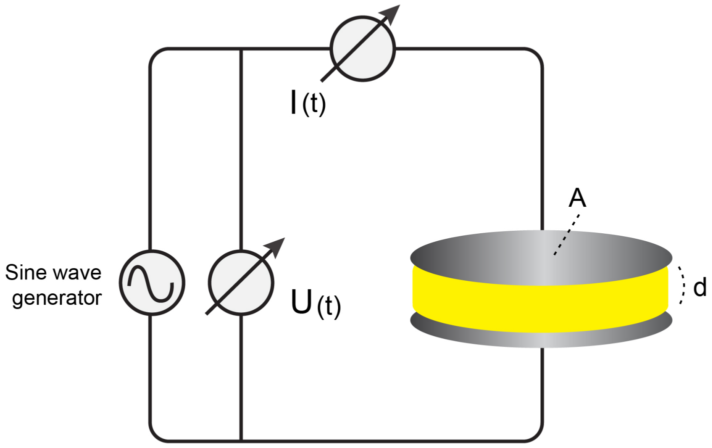

Figure 6.1: Schematic of electric circuit in dielectric spectroscopy

C_0 is the empty cell capacitance and $C_0 = \epsilon_0 A/l$, where A is the area and l is the distance between the electrodes. The impedance can be written as follows:

$$Z^* = \frac{E_s^*}{J_s^*} \tag{6.11}$$

then, the equation (6.12) is given by using the equations (6.9) and (6.10):

$$\epsilon^* = \frac{J_s^*}{iw\epsilon_0 E_s^*} \tag{6.12}$$

Finally, the equation (6.12) can be used to find the ionic conductivity [42]:

$$\frac{J_s^*}{E_s^*} = \sigma^* = iw\epsilon_0\epsilon^* \tag{6.13}$$

6.1.1 Dielectric Relaxation

Dielectric data can be fitted by model functions to determine the relaxation behaviour. Various types of relaxations are identified as α relaxation, β relaxation and γ relaxation.

Debye defined the Debye-equation for an ideal system of polar molecules in gaseous form. In the Debye - relaxation function, the relation between complex permittivity and frequency is described by the equation:

$$\epsilon^*(w) = \epsilon_\infty + \frac{\Delta\epsilon}{1 + iw\tau_D}\ , \quad \Delta\epsilon = \epsilon_s - \epsilon_\infty \tag{6.14}$$

Where $\Delta\epsilon$ expresses the subtraction of the permittivity at high frequency ϵ_∞, from that at the low frequency ϵ_s. τ_D is the characteristic relaxation time. The loss peak has a symmetric shape. Although this model is suitable for small polar molecular liquids which have one specific relaxation time, it cannot predict dielectric spectra of liquids and solid dielectrics correctly, where the reorientation of molecules is a complicated process. This causes a modification of the Debye function to the more general Havriliak-Negami function, which is given by the equation:

$$\epsilon^*(w) = \epsilon_\infty + \frac{\Delta\epsilon}{(1+(iw\tau_D)^\alpha)^\beta}\ , \quad 0 \leq \alpha \leq 1, \quad 0 \leq \beta \leq 1 \tag{6.15}$$

Havriliak-Negami, describing the symmetric and asymmetric broadening of a Debye function. Parameters α and β are between 0-1. In the case of α=1, the so called Cole-Davison (6.16) function is obtained, which represents an asymmetric broadening. This function is commonly used to describe the α relaxation. The Cole-Davidson function is given by

$$\epsilon^*(w) = \epsilon_\infty + \frac{\Delta\epsilon}{(1+iw\tau_D)^\beta}\ , \quad 0 \leq \beta \leq 1 \tag{6.16}$$

and the Cole Cole relation is given by the (6.17) function. It is used to describe the symmetric broadering of the β and γ relaxations.

$$\epsilon^*(w) = \epsilon_\infty + \frac{\Delta\epsilon}{1+(iw\tau_D)^\alpha}\ , \quad 0 \leq \alpha \leq 1 \tag{6.17}$$

In the case of $\alpha = 1$ and $\beta = 1$, the Debye (6.14) function can be found [42-43].

6.1.2 Differential Scanning Calorimetry

Differential scanning calorimetry (DSC) is a preferred method among thermal analytical techniques due to its simplicity, cheap price and reliability. DSC is widely used for investigating and understanding physical and chemical changes of materials. It provides information about energetic properties and makes it possible to study exothermic and endothermic changes, such as melting, crystallization, and glass transition. It probes the energy changes that occur in the molecules during temperature changes. The DSC instrument consists of two pans: a sample and a reference (empty) pan. Generally, pans are made of aluminum alloys, platinum, stainless steel or silver. The sealed sample pan and the reference pan are located on cylindrical platforms in a big furnace, as illustrated in figure 6.2. In this configuration, the sample and reference thermocouples are placed below the platform. The sample and reference are subjected to the heating and cooling (K/min) from the furnace; then, the difference in temperature between the sample and the reference is measured by sensors [44].

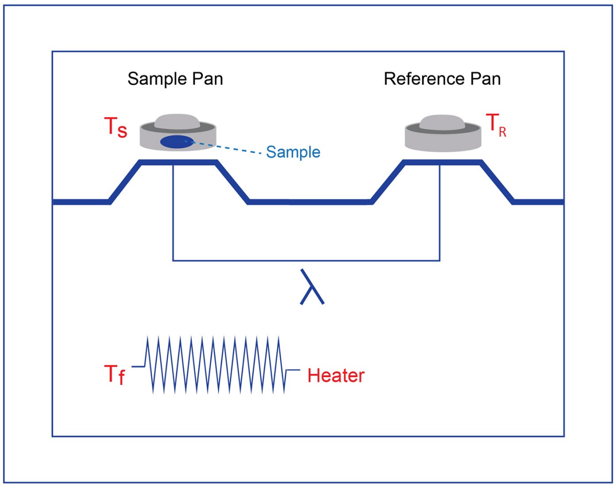

Figure 6.2: Schematic illustration of DSC setup.

The signals received by DSC are given by the heat flow, to or from the sample, to maintain its temperature, and can be defined as follows:

$$\frac{dQ}{dt} = \frac{(T_S - T_R)}{\lambda} \tag{6.18}$$

where dQ/dt is the heat flow, measured in mW, T_S is the sample temperature, T_R is the furnace temperature, and λ is the thermal resistance of the metal disc which connects the pans. Furthermore, DSC measures the heat capacity changes of the sample. The relation between heat flow, heat capacity, and enthalpy can be written as follows:

$$\frac{dQ}{dt} = C_S(\frac{T_S}{dt}) - (\frac{dH}{dt}) \tag{6.19}$$

where C_S is the heat capacity of the sample and H is the sample enthalpy [44-45]. In figure 6.3, glass transition temperature, melting point, and crystallization are shown. Defining the T$_g$, onset, midpoint, and endpoint can be extracted by drawing the tangents to the base line before and after the glass transition, and a tangent of the point with the highest derivative in the transition step.

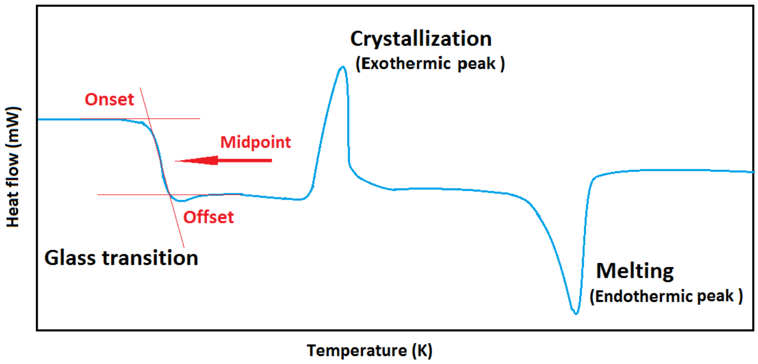

Figure 6.3: DSC thermogram and T_g determination

6.1.3 Thermal Gravimetric Analysis (TGA)

TGA is a thermal analysis technique used to compliment information from other thermal techniques in order to characterize the material. TGA records weight changes of materials (mass losses or gains), as a function of time or temperature, $\Delta m = F\ (T, t)$. A microgram balance continually measures the mass change of the sample, while a furnace supports the heating or cooling. The change in mass can be a result of physical events such as adsorption, desorption, oxidation, decomposition, or dehydration. A thermocouple monitors the temperature of the sample. The sample environment is controlled by a purge gas such as N_2 or H_2. The sample mass is commonly in the range of 20-50 mg. In addition, a large sample area is exposed to the purge gas [46]. The sample pans are usually made from aluminum and platinum. The accuracy of the collected data depends on a number of parameters, such as sample mass, purge gas, and pan type. Data obtained using TGA is recorded as a graph where the change in mass versus temperature or time is plotted. T_i is the initial temperature, where the onset of mass change occurs, and T_f is the final temperature of mass change. Sometimes it is difficult to find the initial and final temperature, therefore, extrapolated values of these points; onset and offset points, T_0, are used. Figure 6.4 shows mass loss versus temperature when the sample is heated.

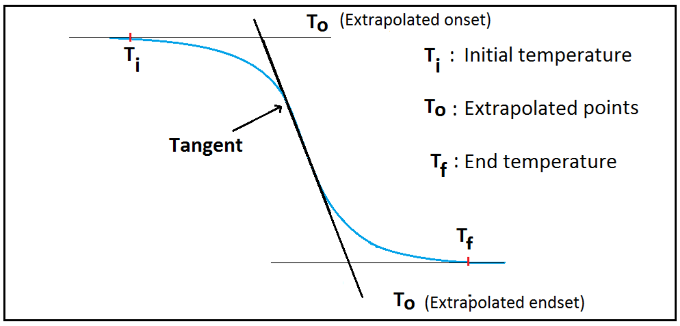

Figure 6.4: Typical TGA curve when mass changes between T$_i$ - T$_f$

6.2 Experimental Conditions

In the following, the conditions during the measurements for all instruments used in this study, *i.e.*, dielectric spectroscopy, differential scanning calorimetry, and thermogravimetric analysis, are described.

6.2.1 Dielectric Spectroscopy Measurements

Dielectric spectra were measured with a Novocontrol broadband dielectric spectrometer, equipped with a Cryo-system (113 K- 673 K), in the frequency range of $10^{-2} - 10^{7}$ Hz; between 135 K and 365 K with a step increment of 5 K. The sample (electrolyte film) was placed in a dielectric cell with electrodes of area 20 mm^2. Figure 6.5 shows the schematic of a sample container in dielectric spectroscopy. The stabilization time between each temperature was set to 600 s.

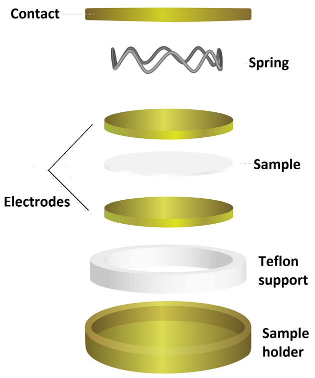

Figure 6.5: Schematic illustration of the dielectric spectroscopy sample container

The results from the measurements were analyzed with the Win Fit software and the α relaxation was fitted by the Cole-Davison function and the β and γ were fitted by the Cole-Cole function. Figure 6.6 shows part of the β and γ relaxation processes in the imaginary part of the permittivity for PEO:LiTFSI- 8:1- 4wt%Al_2O_3 at a temperature of 205 K.

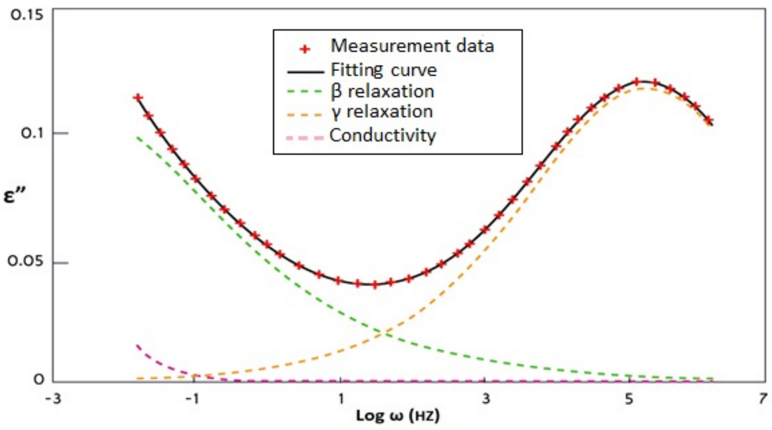

Figure 6.6: experimental data have been fitted by two Cole-Cole functions and a conductivity term.

Figure 6.7 shows conductivity versus frequency for several temperatures of PEO: LiTFSI- 16:1- 4wt%Al_2O_3 (40wt% IL), where the starting point of the almost frequency independent plateau value changes with the temperature. Generally, polarization effects can be found at low frequencies (the conductivity decreases with the decreasing frequency), whereas a.c conductivity can be observed at high frequencies (at the highest frequencies an increasing conductivity is obtained). The plateau region, with a fairly frequency independent conductivity, is observed between these regions. The dc-conductivity was estimated as this plateau value in a conductivity plot.

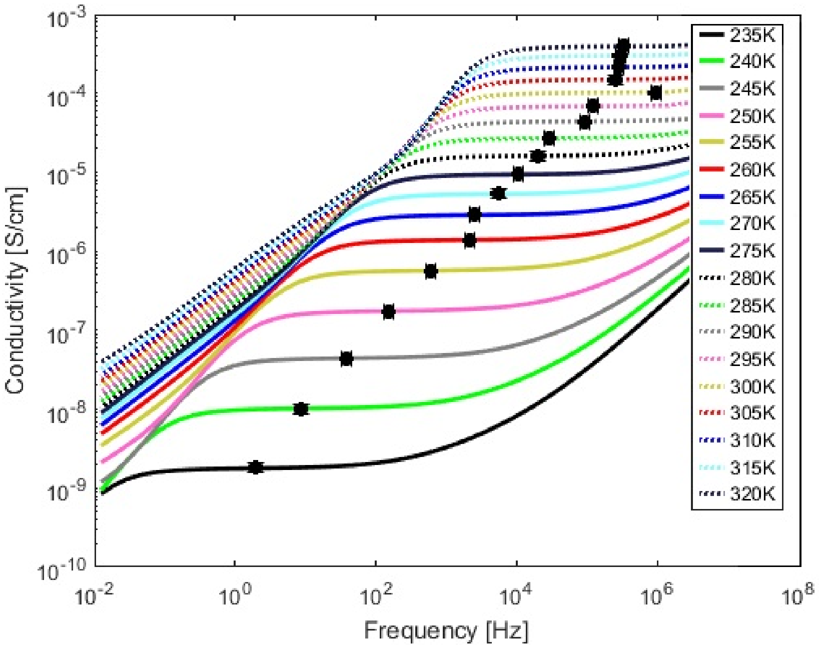

Figure 6.7: Conductivity versus frequency for several temperatures of PEO: LiTFSI- 16:1- 4wt%Al_2O_3 (40wt% IL). The black squares illustrate the dc conductivity obtained from the plateau observed at each temperature.

6.2.2 DSC Measurements

All Differential Scanning Calorimetry measurements were performed using a Q1000 TA instrument. The instrument was equipped with a liquid nitrogen cooling accessory, and helium was used as a purge gas at a flow rate of 25 ml/min.

The sample (polymer electrolytes) films were encapsulated in an aluminum pan inside a glove box. The measurements were carried out in the range 123 K- 423 K in a nitrogen atmosphere. First, the samples were rapidly cooled to 123 K and afterwards heated up to 423 K with a heating rate of 10 K/min. This procedure was repeated three times. It is important to measure the glass transition temperature in this work. The T_g value was defined as the midpoint in the slope of C_p during the heating in the second cycle.

6.2.3 TGA Measurements

The samples were measured using Netzsch209 TG F_1 Iris, which can operate between 283 K and 1273 K, to ensure the elimination of solvent traces. In this instrument, the purge gas is Helium. In this work, the samples had a weight of 10 – 20 mg and an aluminum pan was used as container. The heating rate was 10 K/min from 293 K- 473 K.

7

Results

After receiving the results from TGA, which show that the samples are clear of solvent, further measurements by DSC and DS were made. In the following chapter, the glass transition of the samples with ratios (16:1 and 8:1) of PEO:LiTFSI, blended with various concentrations of ionic liquid, were determined by DSC, and the dynamics related to the α relaxation, β relaxation and γ relaxation were studied by DS. The ionic conductivity of each sample was also measured.

7.1 TGA Measurements

Figure 7.1 shows the weight loss of PEO:LiTFSI- 16:1- 4wt%Al_2O_3 (0-40wt% IL) and figure 7.2 shows the weight loss for PEO:LiTFSI- 8:1- 4wt%Al_2O_3 (0 and 20wt% IL). The curves show mass changes versus temperature. The results from the TGA measurements illustrate that the samples are dry and suitable for measurements. The mass loss observed from the curves is close to one percent.

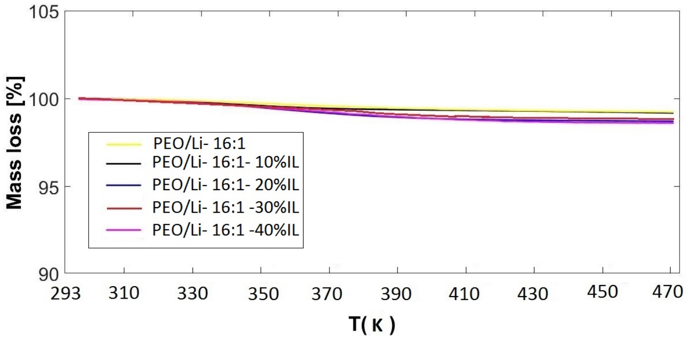

Figure 7.1: TGA weight loss from heating to 473 K at 10 K/min for PEO: LiTFSI-16:1- 4wt%Al_2O_3 ($0 - 40$wt% IL).

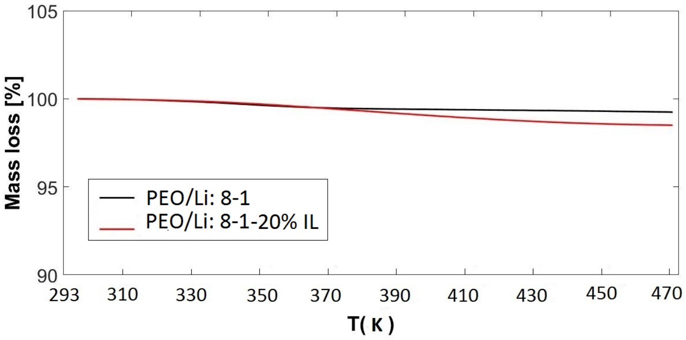

Figure 7.2: TGA weight loss from heating to 473 K at 10 K/min for PEO:LiTFSI-8:1- 4wt%Al_2O_3 (0 and 20wt% IL).

7.2 DSC, PEO-LiTFSI (16:1)-BMITFSI

Figure 7.3 shows the DSC measurements of PEO:LiTFSI- 16:1 during heating. The curves of PEO:LiTFSI- 16:1- 4wt%$Al_2O_3(0-40$wt% IL) and PEO- 4wt%Al_2O_3 are presented in this thermogram. The glass transition can be seen as a discrete change of the baseline. During cooling (not shown), cold crystallization is observed for PEO- 4wt% Al_2O_3, which is due to the semi-crystalline nature of PEO. The PEO-4wt%Al_2O_3 sample exhibits a glass transition at 216K, which is close to the glass transition temperature (T_g) found by previous research [35]. By adding LiTFSI salt, an increase of the T_g can be observed, which is explained by the interaction between the ether oxygens of the PEO chains and the Li ions of the LiTFSI. This interaction decreases the polymer chain flexibility and makes, the polymers stiffer. By blending the ionic liquid with the PEO-LiTFSI, the samples show lower T_g. The T_g which is observed for the sample with 20wt% ionic liquid is 220.3 K. The decrease of the glass transition temperature is interpreted to be caused by the plasticizing effect of the ionic liquid. Small molecules of the ionic liquid facilitate the segmental dynamics of the polymer chains, leading to a lower T_g. However, the addition of higher concentrations of the ionic liquid (30-40 wt%) does not increase the flexibility of the polymer chains further. It appears as a full effect of the ionic liquid for getting faster motions of the polymer, is already obtained at 20 wt% of the ionic liquid. Thus, increasing the concentration of the ionic liquid to over 20 wt% does not reduce the glass transition temperatur further, as shown in table 7.1.

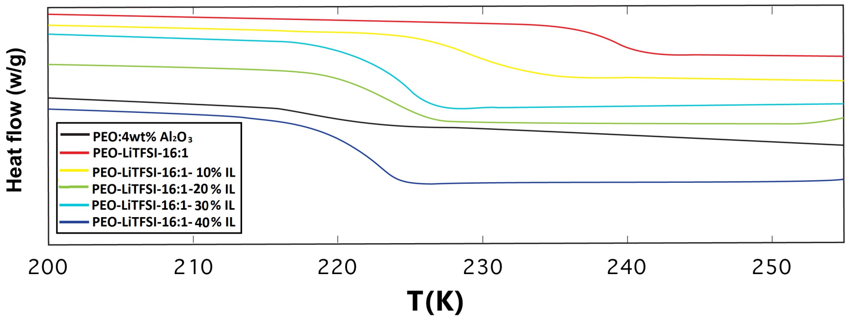

Figure 7.3: DSC thermogram, heat flow versus temperature of PEO:LiTFSI- 16:1- 4wt%Al_2O_3 (0 – 40wt% IL).

Table 7.1: The glass transition temperature for PEO:LiTFSI- 16:1- 4wt%Al_2O_3 with different wt% IL.

Sample (EO/Li 16:1)	T_g
PEO-LiTFSI- 4wt% Al_2O_3	236.4 K
PEO-LiTFSI- 4wt% Al_2O_3 – 10wt% IL	226.7 K
PEO-LiTFSI- 4wt% Al_2O_3 – 20wt% IL	220.3 K
PEO-LiTFSI- 4wt% Al_2O_3 – 30wt% IL	220.8 K
PEO-LiTFSI- 4wt% Al_2O_3 – 40wt% IL	221 K

7.3 DSC, PEO-LiTFSI (8:1)-BMITFSI

Figure 7.4 shows the DSC measurements of PEO-4wt%Al_2O_3 and PEO:LiTFSI -8:1- 4wt%Al_2O_3 with 0 and 20 wt% IL.

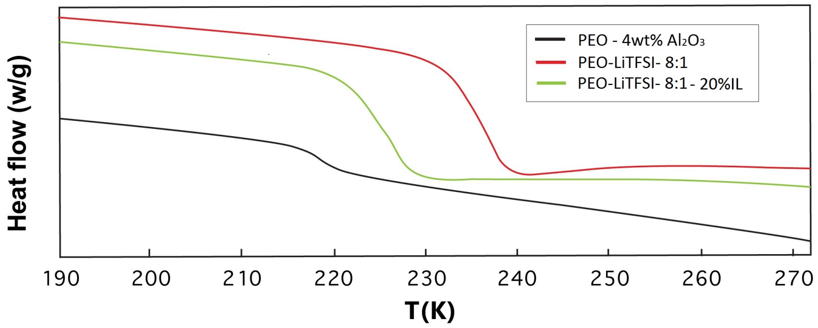

Figure 7.4: DSC curves, Heat flow versus temperature for PEO:LiTFSI- 8:1- 4wt%Al_2O_3 (0 and 20 wt% IL) and PEO- 4wt%Al_2O_3.

As described in section 7;2, by first adding salt to PEO, T_g increases from 216K to 232.5K. Thereafter, the addition of the IL to the PEO:LiTFSI- 8:1- 4wt%Al_2O_3 sample leads to a decrease of T_g to 221.4 K.

Table 7.2: The glass transition temperature for PEO:LiTFSI- 8:1 with 0 and 20wt% IL.

Sample (EO/Li 8:1)	T_g
PEO-LiTFSI- 4wt% Al_2O_3	232.5 K
PEO-LiTFSI- 4wt% Al_2O_3 – 20wt% IL	221.4 K

7.4 Conductivity

The ionic conductivity of the samples with various concentrations of IL is plotted as a function of temperature in Figures 7.5 and 7.6. For different ratios of PEO:LiTFSI, two plots are presented. Figure 7.5 shows the ionic conductivity for PEO:LiTFSI-16:1- 4wt%Al_2O_3 (0 – 40wt% IL). It is observed that the conductivity follows the Vogel–Fulcher–Tammann (VFT) behaviour. As expected, adding higher amounts of the ionic liquid increases the conductivity. The highest conductivity is obtained for the PEO:LiTFSI- 16:1- 4wt%Al_2O_3 (40wt% IL) sample. Thus, the ionic conductivity increases continuously by adding more of the ionic liquid. Since the DSC results showed that T_g and the related segmental polymer dynamics were unaffected by the addition of the ionic liquid above 20wt% IL, this finding implies that motions of the Li^+ ions become decoupled from the segmental polymer dynamics at high concentrations of the ionic liquid.

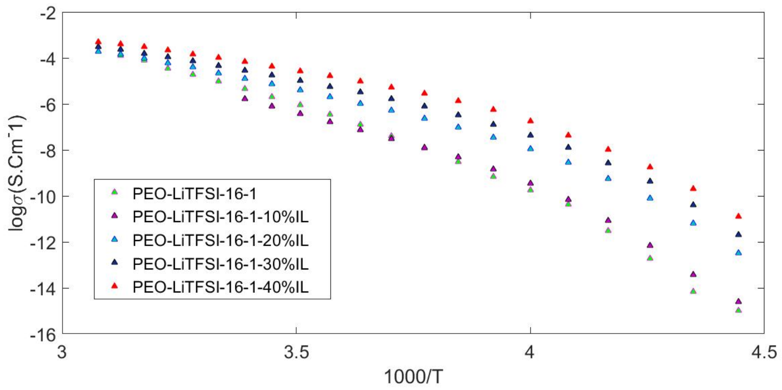

Figure 7.5: Ionic conductivity as a function of inverse temperature for PEO:LiTFSI- 16:1- 4wt%Al_2O_3 (0-40wt% IL).

Figure 7.6 shows the conductivity for samples with PEO:LiTFSI- 8:1. As previously described, the conductivity behaves in a similar way to what was observed in Figure 7.5. The results for samples PEO:Li- 8:1- 4wt%Al_2O_3 (0 and 20wt% IL) show that the addition of an ionic liquid results in higher conductivity, which can be attributed to the ability of the ionic liquid to enhance the ion transfer. The ionic conductivity increases due to a speeding up of the segmental dynamics of the polymer and possibly also due to a decoupling of the Li^+ ions motions from the polymer dynamics, as discussed above. Tables 7.3 and 7.4 show values for ionic conductivity of the polymer electrolyte films PEO:LiTFSI- 16:1- 4wt%Al_2O_3 ($0-40$wt% IL) and PEO:LiTFSI- 8:1- 4wt%Al_2O_3 (0 and 20wt% IL).

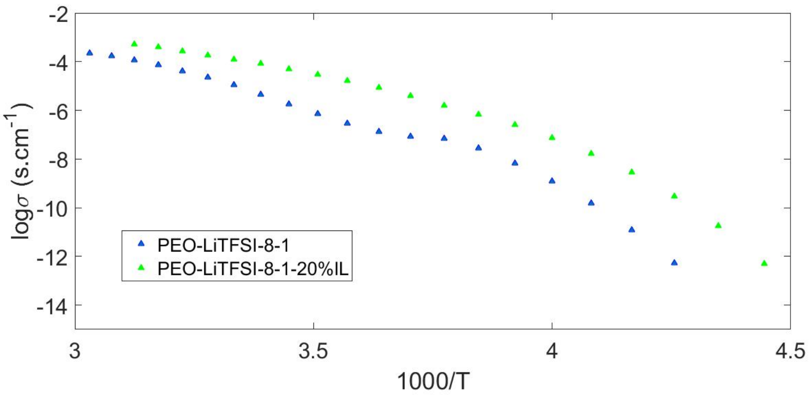

Figure 7.6: Conductivity versus temperature for PEO:LiTFSI- 8:1- 4wt%Al_2O_3 (0 and 20wt% IL).

Table 7.3: The ionic conductivity at room temperature for PEO:LiTFSI- 16:1- 4wt%Al_2O_3 (0-40wt% IL).

Sample (EO/Li) 16:1	Ionic Conductivity, T(300K)/ Scm^{-1}
PEO-LiTFSI- 4wt% Al_2O_3	$9.4 \cdot 10^{-7}$
PEO-LiTFSI- 4wt% Al_2O_3 – 10wt% IL	$1.06 \cdot 10^{-6}$
PEO-LiTFSI- 4wt% Al_2O_3 – 20wt% IL	$2.2 \cdot 10^{-5}$
PEO-LiTFSI- 4wt% Al_2O_3 – 30wt% IL	$4.5 \cdot 10^{-5}$
PEO-LiTFSI- 4wt% Al_2O_3 – 40wt% IL	$1.02 \cdot 10^{-4}$

Table 7.4: The ionic conductivity at room temperature for PEO:LiTFSI- 8:1- 4wt%Al_2O_3 with 0 and 20wt% IL.

Sample (EO/Li) 8:1	Ionic Conductivity, T(300K)/ Scm^{-1}
PEO-LiTFSI- 4wt% Al_2O_3	$1.1 \cdot 10^{-5}$
PEO-LiTFSI- 4wt% Al_2O_3 – 20wt% IL	$1.2 \cdot 10^{-4}$

7.5 Dielectric Relaxations

Figure 7.7 shows the relaxation processes PEO:LiTFSI- 16:1- 4wt%Al_2O_3 (0−40wt% IL), where three types of relaxations, α, β and γ are noted. In semi-crystalline polymers, two relaxation processes, α, β or three relaxation processes, α, β and γ are commonly observed. Each of these processes are defined by their characteristics.

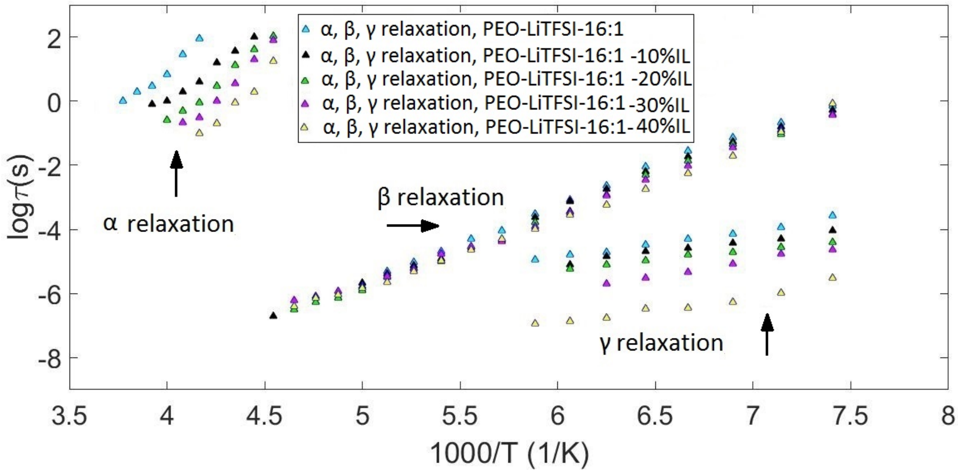

Figure 7.7: Dielectric relaxation times versus temperature for PEO:LiTFSI- 16:1- 4wt %Al_2O_3 (0 – 40wt% IL).

The triangles in the upper left part of figure 7.7 show the α-relaxation time at temperatures above T_g. The mechanism of the α-relaxation is mainly related to segmental motions of the polymer chains. The α-relaxation time decreases by increasing the concentration of the IL. A slight speeding up of the α-relaxation is observed even at concentrations above 20wt% IL. This finding suggests that T_g should continue to decrease in this concentration range, in contrast to the DSC results. However, the speeding up of α-relaxation round T_g is minor.The β-relaxation for PEO:LiTFSI- 16:1- 4wt %Al_2O_3 (0-40 wt% IL) is also shown in figure 7.7 which remains unchanged. The β-relaxation is observed at lower temperatures below T_g

; it is believed to be caused by the movement of the polymer segments close to crystalline regions, in the interphase between amorphous and crystalline regions. It is also proposed that the β-relaxation can be caused by local segmental motions of polymer segments "confined" between ether oxygens coordinated to Li^+ ions [35]. In support for this interpretation is that the strength of the β-relaxation increases with increasing salt content, despite the fact that the crystallinity decreases. Furthermore, in Figure 7.7 the γ-relaxation for PEO:LiTFSI- 16:1- 4wt%Al_2O_3 (0-40 wt% IL) is shown. The γ-relaxation is due to local twistings of chain ends and local intramolecular movements of the ethylene groups. In the figure it is evident that IL makes the γ-relaxation time faster. It is explained by the plasticizering effect of the ionic liquid on the local chain dynamics, which speeds up the relaxation time. Thus, this local polymer motion is facilitated by the presence of the ionic liquid.

Relaxation times of different relaxation processes in PEO:LiTFSI- 8:1 -%Al_2O_3 (0 and 20 wt% IL) are shown in figure 7.8. Also for this salt concentration the β-relaxation time remains unchanged, showing that the concentration of the IL does not affect this "constrained" local segmental relaxation process. Thus, it seems that the β-relaxation is determined by the chain constraints mentioned above (i.e. the bonding to crystalline regions and Li^+ ions), rather than by the non-bonded surrounding. The effect of the ionic liquid on the segmental polymer dynamics and the related α-relaxation is a speeding up in consistency with the decrease in T_g when an ionic liquid is introduced. The exact time scale of the γ-relaxation was difficult to determine, because it mainly occured at frequencies outside of the experimental frequency window.

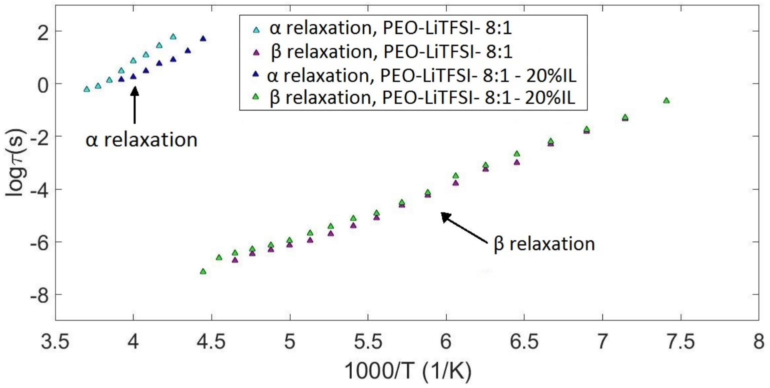

Figure 7.8: Dielectric α and β relaxation times versus temperature for PEO:LiTFSI-8:1- 4wt%Al_2O_3 (0 and 20wt% IL).

8

Conclusion

In this work dielectric relaxation, conductivity and thermal measurements have been used, to study the dynamic properties of the electrolyte films, PEO: LiTFSI- 16:1: 4w%Al_2 O_3 ($0 - 40$wt%IL) and PEO:LiTFSI-8 : 1- 4w% Al_2O_3 (0 and 20wt%IL). PEO is the employed polymer in this study, and when this polymer is mixed with the nanofiller Al_2O_3, a glass transition temperature (T_g) of $216K$ is obtained. This result is in good agreement with T_g that has previously been reported in the literature [35]. Incorporation of the ionic liquid into the electrolyte films (polymer-salt-nanofiller films) shows a reduction of T_g for both salt concentration (8:1 and 16:1). This finding can be explained by the plasticizing effect of the ionic liquid. However, T_g does not change considerably when higher amounts of the ionic liquid ($30 - 40$wt%) are added. The reason for this is that such high concentrations of the ionic liquid do not accelerate the segmental polymer dynamics more than what is already achieved at 20wt% IL. The presence of the ionic liquid also enhances the ionic conductivity. It increases with increasing amount of the ionic liquid for the whole measured concentration range $0 - 40$wt% IL. The increase of the ionic conductivity of up to 20wt%IL seems to be related to an acceleration of the segmental polymer dynamics, which facilitates the motion of the Li^+ ions, while the rise of the ionic conductivity at concentrations above 20wt%IL is likely due to a decoupling of the ionic motions from the segmental polymer dynamics. Instead, the motion of the Li^+ ions seems to be more dependent on the viscosity of the ionic liquid. Based on the experimental results, the highest conductivity is achieved in the PEO:LiTFSI- 8:1- 4wt%Al_2O_3 (20wt% IL) polymer electrolyte film, and is equal to 1.2×10^{-4} S.cm^{-1}. The second highest conductivity is found in PEO:LiTFSI-16:1- 4wt%Al_2O_3 (40wt% IL) with a value of 1.02×10^{-4} S.cm^{-1} . The study of the dynamics of the polymer electrolyte films reveals that the α-relaxation time decreases with an increase of the ionic liquid at least in low concentration range up to 20wt% ionic liquid. The β-relaxation time in different PEO:LiTFSI ratios remains unchanged, due to the fact that the β-relaxation is local in character and not dependent on the amounts of crystallinity and Li^+ coordinated ether oxygens. Only the strength of the β-relaxation depends on these two parameters. The γ-relaxation time, which is related to local twisting of the chain ends, and local stretch movements of ethylene groups, decreases by the addition of the ionic liquid. This can be explanied by the plasticizing effect of the ionic liquid. In order to improve the polymer electrolyte films and to receive the desired properties further complementary studies are required. The study of PEO:LiTFSI- 8:1- 4wt%Al_2O_3 (20wt% IL) shows that the electrolyte film is totally amorphous with a low T_g equal to 221.4 K. The conductivity of this polymer film at room temperature is high. Therefore, this polymer film has the potential to be used as solid electrolyte in future batteries. It is possible that an even higher amount of the IL results in an even higher ionic conductivity and lower glass transition temperature. Moreover, the ionic conductivity and glass transition temperature of PEO:LiTFSI compositions of different PEO:LiTFSI ratios could be interesting to investigate. A study comparing the relaxation times of the pure ionic liquid and the relaxation data presented in this thesis would also be worth investigating further to elucidate whether the ionic liquid may contribute to the β and/or γ-relaxations.

Bibliography

[1] Chu, S., Majumdar, A. *Opportunities and challenges for a sustainable energy future.* nature, 488(7411), 294-303 (2012).

[2] Hadjipaschalis, I., Poullikkas, A., Efthimiou, V. *Overview of current and future energy storage technologies for electric power applications.* Renewable and sustainable energy reviews, 13(6), 1513-1522 (2009).

[3] Tarascon, J. M. and Armand, M. *Issues and challenges facing rechargeable lithium batteries.* Nature, 414(6861), 359-367 (2001).

[4] Li, Q., Chen, J., Fan, L., Kong, X.,Lu, Y. *Progress in electrolytes for rechargeable Li-based batteries and beyond.* Green Energy and Environment (2016).

[5] Li, J., Zhu, H., Wang, X., MacFarlane, D. R., Armand, M. *Increased ion conduction in dual cation [sodium][tetraalkylammonium] poly [4-styrenesulfonyl (trifluoromethylsulfonyl) imide-co-ethylacrylate] ionomers.* Journal of Materials Chemistry A, 3(39), 19989-19995 (2015).

[6] Quartarone, E., Mustarelli, P. *Electrolytes for solid-state lithium rechargeable batteries: recent advances and perspectives.* Chemical Society Reviews, 40(5), 2525-2540 (2011).

[7] Yoshino, A. *the Birth of the Li- Ion Battery.* Angewandte Chemie International. Edition 51. 24, 5798-5800 (2012).

[8] Nishi, Y. *Lithium ion secondary batteries; past 10 years and the future.* Journal of Power Sources 100.1, 101-106 (2001).

[9] Monti, D. *Innovative Electrolytes for Safer Sodium-Ion Batteries.* Ph.D. thesis, Chalmers University of Technology (2016).

[10] Jones, R. AL. *Soft condensed matter.* Vol. 6. Oxford University Press (2002).

[11] Alegria, A., et al. *alpha.-Relaxation in the Glass Transition Range of Amorphous Polymers. 1. Temperature Behavior across the Glass transition.* Macromolecules 28.5, 1516-1527 (1995).

[12] Shujahadeen ,A. B. *Li- ion conduction mechanism in poly (ϵ -caprolactone) based polymer electrolyte.* Iranian Polymer Journal 22.12, 877-883 (2013).

[13] Agrawal, R. C., and G. P. Pandey. *Solid polymer electrolytes: materials designing and all-solid-state battery applications: an overview.* Journal of Physics D: Applied Physics 41.22, 223001 (2008).

[14] Di Noto, Vito, et al. *Polymer electrolytes: Present, past and future.* Electrochimica Acta 57, 4-13 (2011).

[15] Meyer, W . H. *polymer electrolytes: lithium-ion batteries.* Advanced materials 10.6, 439-448 (1998).

[16] Armand, M.B., Bruce, P.G., Forsyth, M., Scrosati, B., Wieczorek, W. *Polymer electrolytes.* Energy Materials, 1-31 (2011).

[17] Zhang, R., et al. *Advanced gel polymer electrolyte for lithium-ion polymer batteries.* Fuel Cell Science, Engineering and Technology. American Society of Mechanical Engineers (2013).

[18] Stephan, A. M. *Review on gel polymer electrolytes for lithium batteries.* European Polymer Journal 42.1, 21-42 (2006).

[19] Michael, M. S., et al. *Enhanced lithium ion transport in PEO-based solid polymer electrolytes employing a novel class of plasticizers.* Solid State Ionics 98.3, 167-174 (1997).

[20] Gondaliya, N., Kanchan, D. K., Sharma, P. *Effect of a plasticizer on a solid polymer electrolyte.* Soc Plast Eng. doi, 10, 2417 (2013).

[21] Wieczorek, W., Florjanczyk, Z., Stevens, J. R. *Composite polyether based solid electrolytes.* Electrochimica Acta, 40(13), 2251-2258 , (1995).

[22] Croce, F., et al. *Nanocomposite polymer electrolytes for lithium batteries.* Nature 394.6692,456-458 (1998).

[23] Wieczorek, W., Florjanczyk, Z., Stevens, J. R. *Composite polyether based solid electrolytes.* Electrochimica Acta, 40(13), 2251-2258 (1995).

[24] Wilken, S. *Failure Mechanisms of Lithium-ion Battery Electrolytes: Detection and Mitigation.* Ph.D. thesis, Chalmers University of Technology (2014).

[25] Wieczorek, W., Florjanczyk, Z., Stevens, J. R. *Composite polyether based solid electrolytes.* Electrochimica Acta,40(13), 2251-2258 (1995).

[26] Markusson, H. *New Electrolyte Materials for Lithium Batteries and Fuel Cells-an ab initio and vibrational spectroscopy study.* Ph.D. thesis, Chalmers University of Technology (2006).

[27] Adebahr, J. *Molecular Interactions and Dynamics in Lithium Conducting Electrolytes.* Ph.D. thesis, Chalmers University of Technology (2002).

[28] Ghandi, Kh. *A review of ionic liquids, their limits and applications.* Green and Sustainable Chemistry 2014 (2014).

[29] Lee, B. C., Outcalt, S. L. *Solubilities of gases in the ionic liquid 1-n-butyl-3-methylimidazolium bis (trifluoromethylsulfonyl) imide.* Journal of Chemical and Engineering Data, 51(3), 892-897 (2006).

[30] Kim, J. K. *Advanced Materials for Rechargeable Lithium Batteries.* Ph.D. thesis, Chalmers University of Technology (2012).

[31] Chaurasia, S. K., Singh, R. K., Chandra, S. *Effect of ionic liquid on the crystallization kinetics behaviour of polymer poly (ethylene oxide).* CrystEngComm,15(30), 6022-6034 (2013).

[32] Ahn, J. H., Wang, G. X., Liu, H. K., Dou, S. X. *Nanoparticle-dispersed PEO polymer electrolytes for Li batteries.* Journal of power sources, 119, 422-426 (2003).

[33] Jayathilaka, P. A. R. D., Dissanayake, M. A. K. L., Albinsson, I., Mellander, B. E. *Effect of nano-porous Al 2 O 3 on thermal, dielectric and transport properties of the (PEO) 9 LiTFSI polymer electrolyte system.* Electrochimica acta, 47(20), 3257-3268 (2002).

[34] Michael, M. S., Jacob, M. M. E., Prabaharan, S. R. S., Radhakrishna, S. *Enhanced lithium ion transport in PEO-based solid polymer electrolytes employing a novel class of plasticizers.* Solid State Ionics, 98(3), 167-174 (1997).

[35] Money, B. K., Hariharan, K., Swenson, J. *Glass transition and relaxation processes of nanocomposite polymer electrolytes.* The Journal of Physical Chemistry B,116(26), 7762-7770 (2012).

[36] Keller, A. *Crystalline polymers; an introduction.* Faraday Discussions of the Chemical Society, 68, 145-166 (1979).

[37] Ebewele, R. O. *Polymer science and technology.* CRC press (2000).

[38] Bailey, F. J. *Poly(ethylene oxide)*, Elsevier (2012).

[39] Marzantowicz, M., Dygas, J. R., Krok, F., Łasińska, A., Florjańczyk, Z., *Crystallization and melting of PEO: LiTFSI polymer electrolytes investigated simultaneously by impedance spectroscopy and polarizing microscopy.* Electrochimica acta, 50(19), 3969-3977 (2005).

[40] Choi, J. W., Cheruvally, G., Kim, Y. H., Kim, J. K., Manuel. *Poly (ethylene oxide)-based "polymer electrolyte incorporating room-temperature ionic liquid for lithium batteries.* Solid State Ionics, 178(19), 1235-1241 (2007).

[41] Blythe, A. R., Bloor, D. *Electrical properties of polymers.* Cambridge University Press (2005).

[42] Ahmad, Z. *Polymeric dielectric materials.* Dielectric Material, 3-26 (2012).

[43] Kremer F., Schönhals A., *Broadband Dielectric Spectroscopy.* Springer-Verlag, Berlin Heidelberg (2003).

[44] Leys, J. *Broadband dielectric spectroscopy of confined liquid crystals and hydrogen bonded liquids*, (2007).

[45] Haines, P. J. *Principles of thermal analysis and calorimetry.* Royal society of chemistry (2002).

[46] Gabbott, P. (Ed.). *Principles and applications of thermal analysis.* John Wiley Sons (2008).

[47] Brown, M. E., Gallagher, P. K. *Handbook of thermal analysis and calorimetry: recent advances.* techniques and applications (Vol. 5). Elsevier (2011).